Atmospheric CO2 flux and planktonic food web relationships in temperate marsh systems: Insights from in situ water measurements

Xaus Lucila

lucila.xaus@univ-lr.fr

LIENSs, UMR7266 CNRS- La Rochelle Université

Moncelon Raphaël

LIENSs, UMR7266 CNRS- La Rochelle Université

Mayen Jérémy

Ifremer, LITTORAL, F-17390 La Tremblade

Bergeon Lauriane

LIENSs, UMR7266 CNRS- La Rochelle Université

Dubillot Bénédicte

LIENSs, UMR7266 CNRS- La Rochelle Université

Pineau Philippe

LIENSs, UMR7266 CNRS- La Rochelle Université

Emery Claire

LIENSs, UMR7266 CNRS- La Rochelle Université

Vagner Marie

Ifremer/PFOM/ARN, UMR LEMAR 6539, 29280 Plouzané

Robin Francois-Xavier

UNIMA, Union des Marais de la Charente-Maritime

Azémar Frédéric

Laboratoire écologie fonctionnelle et environnement /CNRS-Université de Toulouse

Tackx Michèle

Laboratoire écologie fonctionnelle et environnement /CNRS-Université de Toulouse

Dupuy Christine

LIENSs, UMR7266 CNRS- La Rochelle Université

Polsenaere Pierre

Ifremer, LITTORAL, F-17390 La Tremblade

Research Article

Abstract

While research has extensively investigated the dynamics of CO_2 water partial pressure (pCO_2) and planktonic food webs (PFWs) separately, there has been limited exploration of their potential interconnections, especially in marsh typologies. This study's objectives were to (1) investigated if pCO_2 and atmospheric CO_2 flux can be elucidated by PFW topologies, and (2) ascertain if these potential relationships are consistent across two distinct "Blue Carbon" ecosystems. Abiotic and biotic variables were measured in two contrasting wetlands at the Atlantic French coast: a saltwater (SM, L'Houmeau) and a freshwater marsh (FM, Tasdon). SM acted as a weak carbon source, with pCO_2 between 542 and 842 ppmv. Conversely, FM exhibited strong atmospheric CO_2 source or sink characteristics, varying with seasons and stations, with pCO_2 between 3201 and 114 ppmv. Five PFW topologies were linked to varying pCO_2 across the two ecosystems: three stable topologies ('biological winter', 'microbial', 'multivorous' PFW) exhibited consistently high pCO_2 values (FM: 971, 1136, 3020 ppmv; SM: 'biological winter' not observed, 842, 832 ppmv), while two transient topologies ('weak multivorous' and 'weak herbivorous') displayed lower and more variable pCO_2 values (FM: from 127 to 1402 ppmv; SM: from 638 to 749 ppmv). Seasonality emerged as an influencing factor for both pCO_2 dynamics and PFW. However, PFW in FM did not demonstrate a seasonal equilibrium state, potentially hindering a clearer understanding of the relationship between pCO_2 and PFW. This is the first documented association between PFW topologies and pCO_2 dynamics in "Blue Carbon" marsh environments.

1. Introduction

For decades, atmospheric CO_2 emissions have surged due to human activities like heavy reliance on fossil fuels, deforestation, and agriculture (Canadell et al. 2021). Consequently, extensive research has been dedicated to this issue. Accurately assessing anthropogenic CO_2 emissions and their redistribution among the atmosphere, ocean, and terrestrial biosphere in a changing climate is critical for deciphering regional and global carbon cycles, predicting future climate changes, and formulating effective climate policies (Friedlingstein et al. 2022).

Over short time spans, CO_2 partial pressure (pCO_2) in the atmosphere remains relatively stable (Takahashi et al. 2002). However, in surface waters, it can fluctuate dramatically spatially and temporally, varying by more than four orders of magnitude (Sobek, Tranvik, and Cole 2005; Takahashi et al. 2002). Calculating atmospheric CO_2 fluxes involves assessing the disparity between surface water and atmospheric pCO_2 levels (Mayen et al. 2023; Polsenaere et al. 2023; Takahashi et al. 1997). These fluxes undergo changes influenced by both the water-air pCO_2 gradient and the nature of the water mass (freshwater vs. seawater). Various physical factors (e.g., temperature, winds, surface water mixing) and biological processes (e.g., $CaCO_3$ dissolution/precipitation, primary production, and respiration) influence water pCO_2 (Fig. 1) (Moreau et al. 2013). Nonetheless, Dai et al. (2009) found that in other coastal systems, such as marshes, the strong relationship between oceanic CO_2 flux and temperature appears to be influenced by factors other than temperature. This indicates a significant biological control on water

pCO_2, along with the effects of horizontal advection and water-sediment exchanges in these shallow land-sea interface ecosystems (Mayen et al. 2023).

In this context, coastal vegetated systems such as salt marshes, seagrass meadows, and mangroves are recognized for their main role in "Blue Carbon" sequestration and storage (Chmura et al. 2003; C. M. Duarte, Middelburg, and Caraco 2005; Greiner et al. 2013; Macreadie, Nielsen, et al. 2017; Macreadie, Serrano, et al. 2017; Mcleod et al. 2011), with an average sequestration rate of over 200 ± 24 g C m^{-2} yr^{-1} (Mcleod et al. 2011). Specially, the La Rochelle metropolitan area in France (Fig. 2-A, B) contains nearly 25,580 hectares of wetlands, accounting for almost 45% of its surface area (Afonso 2023). These wetlands have garnered attention from researchers studying their carbon dynamics through *in situ* measurements of water pCO_2 (Mayen et al. 2023), Eddy Covariance (EC) measurements of atmospheric CO_2 exchanges (-483 g C m^{-2} yr^{-1} saltwater marsh storage capacity (Mayen et al. 2024)), and sediment analysis (up to -345 g C m^{-2} yr^{-1} in high carbon sequestration rates (Amann et al. 2023)). Coastal marshes can vary in structure depending on their location; they may be connected to inland rivers, include a dam, or be linked to the sea, such as the studied freshwater marsh (Tasdon) (Fig. 2-B, D). Additionally, these marshes may be managed by humans for activities such as shellfish farming and agriculture, as seen in the L'Houmeau saltwater marsh used in this study (Fig. 2-B, C)). Furthermore, the physical characteristics and biota of marshes are site-specific, influenced by tidal regimes, exposure to wind and waves, and sediment supply (Fagherazzi et al. 2013).

Primary production can increase or decrease depending on various factors, including the phytoplankton cell size (Sieburth, Smetacek, and Lenz 1978), the biomass of autotrophic organisms, specific photosynthetic activity, and several abiotic factors such as temperature, light availability, and nutrient concentrations (Fig. 1). Shiomoto (1997) found that in the Okhotsk Sea, small-sized nano- (2 to 20 μm) and pico- (0.2 to 2 μm) phytoplankton could contribute up to 70% of primary production. On the Atlantic coast of France (Fig. 2-A), Moncelon et al. (2022) proposed that microphytobenthos, along with pico- and nanophytoplankton, may significantly contribute to the total primary production in freshwater marshes. Del Giorgio and Williams (2005) suggested that in general coastal ecosystems, mesozooplankton consume between 12 and 35% of primary production daily, while microzooplankton graze between 60 and 75%. Additionally, heterotrophic prokaryotes respiration often exceeds primary production in aquatic ecosystems (Del Giorgio, Cole, and Cimbleris 1997). These findings underscore the importance of studying planktonic food web (PFW) topologies to better understand their ecological and biological behavior in wetlands, as well as the CO_2 emissions associated with them.

PFWs have been extensively described in marine and coastal areas (Legendre and Rassoulzadegan 1995; Legendre and Rivkin 2005). On the west coast of France (Fig. 2-A), the functional role of the 'microbial food web' in marshes has been detailed by Dupuy et al. (1999, 2011), along with the relationship between PFW dynamics and phytoplankton blooms on the continental shelf (Marquis et al. 2007). Recent studies focusing on marshes (Bergeon et al. 2023; Masclaux et al. 2014; Tortajada 2011) have defined five main PFWs: 'herbivore', 'multivorous, 'microbial food web', 'microbial loop', and 'biological winter', each presenting different degrees of PFW nuances (Tortajada 2011). Furthermore, studying PFWs has proven

invaluable for understanding ecosystem functioning (Beaugrand 2005; Masclaux et al. 2014; Vincent, Luczak, and Sautour 2002). As previously mentioned, water pCO_2 variations in costal ecosystems are greatly influenced by biological activities (Mayen et al. 2024; Moreau et al. 2013). Only a few studies have focused on the relationships between food webs and carbon exchange. Notable examples include Berg et al. (2019), Mayen et al. (2024) and Polsenaere et al. (2013), which examined the links between atmospheric CO_2 flux, water pCO_2 dynamics, and the metabolism of benthic seagrass and marsh plants. Additionally, planktonic communities in coastal marshes seem to play a purifying role by retaining suspended matter, nutrients, and pollutants in the water column, helping to prevent eutrophication (Azim et al. 2005; Nyman 2011; Verhoeven et al. 2006).

Even though, both PFW topologies and the CO_2 cycle have been broadly studied in coastal zones, few studies have examined their association (Legendre and Rivkin 2005; Moreau et al. 2013; Niquil et al. 2006), particularly in diverse marsh (Adamczyk and Shurin 2015; Masclaux et al. 2014). Consequently, much about the relationship between PFWs and water CO_2 in marshes remains unknown.

The aim of this study is to (1) investigate whether variations in pCO_2 and atmospheric CO_2 flux can be explained by PFWs, and (2) determine if the potential relationships between PFWs and water CO_2 exchanges are consistent across two contrasting "Blue Carbon" ecosystems. To address these objectives, monthly samplings were conducted in 2021 in a saltwater marsh (L'Houmeau marsh; Fig. 2-C), and seasonal samplings in a restored freshwater marsh (Tasdon; Fig. 2-D). Abiotic and biotic variables were monitored alongside simultaneous water pCO_2 measurements and atmospheric CO_2 flux estimations, leading to the first known relationships between PFW topology and water pCO_2 in temperate marshes.

2. Materials and Methods

2.1. Overview of the studied marsh sites

The L'Houmeau saltwater marsh (SM) is a salt pond (basin) located behind a dike and originally used for oyster farming on the north side of La Rochelle city (Atlantic coast, France) (Fig. 2-B, C). The studied basin, which is 10 meters wide and 1.5 meters high at the top, naturally fills when the tide range exceeds 60 cm, reaching a maximum volume of 270 m^3. A mechanical valve system manages the inflow and outflow of saltwater from the sea (Fig. 2-C, a, b). For this study, the water volume fluctuated between 90 and 144 m^3, corresponding to a basin fill level between 0.50 and 0.80 meters, respectively. Both biotic and abiotic data monitored at this site are described in Moncelon (2022) and are briefly presented in sections 2.2. and 2.3.

The Tasdon freshwater marsh (FM) is a shallow wetland spanning 123 hectares, located within the urban area of La Rochelle (Fig. 2-B, D, a). From 2019 to 2021, a restoration process was undertaken to reconnect the marsh with the coastal ocean. This restoration included replanting 63,000 aquatic plants and adding sediment to reshape the sediment stock at three stations. This peri-urban marsh is influenced by different water inputs from both the Atlantic Ocean through the Pertuis Sounds and river discharges (Fig. 2-D).

Biotic and abiotic data monitored at this site are briefly presented in sections 2.2. and 2.3, and described in detail by Bergeon et al. (2023) and Mayen (2024). Additionally, the research is associated with several projects: PAMPAS (2019−2024, Evolution de l'identité PAtrimoniale des Marais des Pertuis charentais en réponse à l'Aléa de Submersion marine), Dycidemaim (LEFE 2021−2022, Dynamique du carbone aux interfaces d'échange terrestre-aquatique-atmosphérique des marais tempérés), and LRTZC (2019−2027, La Rochelle territoire zéro carbone).

2.2. Abiotic parameter samplings

At the SM, measurement samplings were conducted monthly between March and August 2021 (Table 1). Over 90% of the water column was refreshed monthly by the mechanical valve system (Fig. 2-C, b), with an adjustment period of 2−3 days before the start of samplings. The remaining 10% above the sediment helped minimize disturbance of the sediment-water interface. At the FM, seasonal samplings were carried out in the years of 2021 and 2022, following the marsh restoration, at three different stations: one with no direct water input (TA), one with direct river discharges (TB), and one with oceanic influence (TC) (Table 1, Fig. 2-D).

Table 1
Samples and measurement methods for the saltwater (SM, L'Houmeau) and freshwater (FM, Tasdon) marshes. Abiotic parameters: Temperature, Salinity, Turbidity, O_2%, Wind gust, pCO_2 (water CO_2 partial pressure), CO_2 flux, Nutrients (NO_3^-, NO_2^-, NH_4^+, PO_4^{3-}, Si) and DOC (dissolved organic carbon). Biotic parameters; Chl$a$ (Chlorophyll-a), Meso (mesozooplankton), Micro (microzooplankton), Proto (heterotrophic protozoan), HTTP (heterotrophic prokaryotes). Sampling periods are mentioned at the bottom of the table

	Temperature (°C)	Salinity	Turbidity (NTU)	O_2%	Wind gust ($m^{-1} s^{-1}$)	pCO_2 (ppmv)	CO_2 flux (mmol $m^{-2} h^{-1}$)
SM	YSI sensor (continuous) + VWR multimeter (discrete)				Infoclimat.fr	C-Sense probe, 24h, measured every minute	Estimation (see Polsenaere et al. (2023))
FM	YSI sensor (continuous)				Infoclimat.fr	C-Sense probe, 24h, 3 days, measured every minute	Estimation (see Polsenaere et al. (2023))

	Nutrients ($\mu mol\ L^{-1}$)	DOC ($mg\ L^{-1}$)
	Triplicated	Triplicated
SM	SEAL AA3 autoanalyzer	Standard NF EN 1484
FM	SEAL AA3 autoanalyzer	-

	Chl$a$ ($\mu g\ L^{-1}$)	Meso (ind m^{-3})	Micro (ind m^{-3})	Proto (ind L^{-1})	HTTP (ind mL^{-1})
	Triplicated	Triplicated	Triplicated		Triplicated
SM	Filters: 20 μm, later 3 μm and 0.7 μm	Filters: 200 μm	-	-	Flow cytometry analysis
FM	Filters: 20 μm, later 3 μm and 0.7 μm	Filters: 200 μm	Filters: 63 μm	Flowcam analysis	Flow cytometry analysis

	Chla	Meso	Micro	Proto	HTTP
	Carbon biomass ($\mu gC.L^{-1}$)				
SM	50[a]	1.44 (ind L^{-1})[b]	-	-	*14 (fgC $cell^{-1}$) [e]

	Temperature (°C)	Salinity	Turbidity (NTU)	O_2%	Wind gust ($m^{-1}\,s^{-1}$)	pCO_2 (ppmv)	CO_2 flux ($mmol\,m^{-2}\,h^{-1}$)
FM	50[a]	0.768 to 1.44 (ind L^{-1}) [b]		0.028 (ind L^{-1}) [b]		2318 (cil) (pgC cell^{-1}) [c], 225 (din) (pgC cell^{-1}) [d]	*14 (fgC cell^{-1}) [e]

Conversion factors used: [a](Tilzer and Dubinsky 1987); [b](Dumont, Van de Velde, and Dumont 1975); Ciliates (cil): [c] (Putt and Stoecker 1989); Dinoflagelates (din): [d](Fournier et al. 2012); [e](Gundersen et al. 2002).

Abiotic and water CO_2 measurement dates: FM: Spring: April 13th to 15th, Summer: August 16th to 18th, Autumn: December 13th to 15th, 2021, Winter: March 1st to 3rd, 2022; SM: March 17th, April 14th, May 18th, June 14th, July 15th, August 9th, 2021.

Nutrients, DOC and biotic sampling dates: FM: Spring: April 15th, Summer: August 25th, Autumn: November 16th, 2021, Winter: March 9th, 2022; SM: March 18th, April 14th, May 19th, June 13th, July 15th, August 9th, 2021.

For both the SM and the FM, several parameters were measured continuously (one measurement every 15 minutes) in subsurface waters (at 0.50 meters below the surface) using an EXO2 multiparameter probe (YSI) with a precision of ± 0.1°C for temperature, ± 0.5 µS cm⁻¹ for salinity/conductivity, ± 0.3 NTU for turbidity, ± 3.1 µmol L⁻¹ for dissolved oxygen concentration, and ± 1% for oxygen saturation percentage (%) (Table 1). Additionally, discrete measurements (once a month) of water temperature, salinity, and dissolved oxygen were taken with a VWR multimeter.

An autonomous pCO_2 underwater probe (C-Sense™ pCO_2 sensor, PME/Turner Designs) with a range of 0-2000 ppmv and a precision of 3% of the range, along with a miniPAR logger (PME), were utilized to measure water pCO_2 and water Photosynthetic Active Radiation (PAR), respectively, continuously (per minute) over a 24-hour period (Table 1) (Mayen et al. 2023). Water-air CO_2 fluxes were estimated following the methodology described in Mayen et al. (2023) and Polsenaere et al. (2023). The CO_2 transfer coefficients, normalized to a Schmidt number of 600 and obtained from Raymond and Cole (2001), were converted to the gas transfer velocity at the *in situ* temperature following (Jähne, Heinz, and Dietrich 1987). The non-temperature ($NpCO_2$) and temperature ($TpCO_2$) effects on diurnal pCO_2 variations were calculated as described by Takahashi et al. (2002) and applied to the marsh ecosystems as done in Mayen et al. (2023) and shown in Eqs. (1) and (2). $TpCO_2$ is related to the physical effects of temperature on water pCO_2 (physical pump, Fig. 1), while $NpCO_2$ corresponds to pCO_2 variations related to other effects, such as biological processes, tidal advection, and water-sediment exchanges, which are particularly important in nearshore costal systems (Mayen et al. 2023).

$$TpCO_2 = pCO_{2mean} \times exp[0.0423 \times (T_{obs} - T_{mean})] \quad (1)$$

$$NpCO_2 = pCO_{2obs} \times exp[0.0423 \times (T_{mean} - T_{obs})] \quad (2)$$

where T_{obs} and pCO_{2obs} represent mean of the observed temperature and pCO_2 values, respectively, measured every minute by the probes. T_{mean} and pCO_{2mean} refer to the seasonal (annual mean) or diurnal (mean per 24-hour cycle) average values.

The CO_2 flux was calculated following the methodology outlined by Polsenaere et al. (2023) and Ribas-Ribas, Gómez-Parra, and Forja (2011), as represented in Eq. (3):

$$FCO_2 = \alpha \times k \times \Delta pCO_2 \quad (3)$$

where FCO_2 (mmol m^{-2} h^{-1}) represents the estimated air–water CO_2 fluxes, where α (mol kg^{-1} atm^{-1}) is the CO_2 solubility coefficient in saltwater, k (cm h^{-1}) denotes the transfer velocity of CO_2 gas, and ΔpCO_2 (ppmv) is the difference between water and air pCO_2 means. For further details on CO_2 flux estimation and C-Sense probe calibration, please refer to Mayen et al. (2023) and the other references cited above.

At both sites, surface water samples were collected in triplicates to measure concentrations of inorganic nutrients and dissolved organic carbon. The methodology outlined by Aminot and Kerouel (2007) and Aminot and Kérouel (2004) was followed to determine nutrient concentrations (nitrate (NO_3^-), nitrite (NO_2^-), ammonium (NH_4^+), phosphate (PO_4^{3-}) and silicate (Si)) in filtered water (0.7 μm GF/F glass fiber membrane, Whatman) using a SEAL AA3 autoanalyzer. The detection limit was 0.02 μmol L^{-1} (Aminot and Kerouel 2007). Dissolved organic carbon (DOC, mg L^{-1}) concentrations were only measured at the SM and were determined by the QUALYSE laboratory following standard NF EN 1484 (Table 1).

2.3. Sampling of biotic parameters

At both the SM and the FM, biotic parameters were systematically monitored in triplicates during the day, on a monthly basis (between March and August 2021) at SM and seasonally throughout 2021 and 2022 at FM (Table 1). Chlorophyll-a (Chl*a*) biomass in different phytoplankton size classes was quantified by collecting surface water samples and following the method outlined by Yentsch and Menzel (1963). This involved sequential filtration through 20 μm (micro), 3 μm (nano), and 0.7 μm (pico) filters (Table 1).

During each sampling period, metazoan mesozooplankton (Meso) abundance was assessed using a 200 μm mesh size net (WP2 plankton net), and its abundance was measured in individuals per cubic meter (ind m^{-3}). Metazoan microzooplankton (Micro) abundance was determined at the FM by filtering 6 L of water through a 63 μm mesh size net (Table 1). Abundance of heterotrophic prokaryotes (HTTP) was measured by flow cytometry of a 1.5 mL water sample according to Marie et al. (1999), while heterotrophic protozoan abundance (Proto) was measured using Flowcam (Buskey and Hyatt 2006). Primary production (PP) by size class (pico, nano, and micro, in mg C m^{-3} h^{-1}) was exclusively measured

at the SM using Nielsen (1951) radioactivity protocol (Table 1). For more detailed information regarding identification and measurement methodologies, please see Bergeon et al. (2023) and Moncelon (2022).

2.4. Statistical analysis

Statistical analysis was conducted using R software (version 4.2.3). Given that the data did not adhere to a normal distribution (Shapiro-Wilk, p-value < 0.05), non-parametric tests were employed for exploratory analysis. Specifically, the rstatix package (Kassambara 2019), and ggbreak package (Xu et al. 2021) were utilized. Differences in Chl*a* biomass, PP by size class, HTTP, Meso abundance (as well as Micro and Proto in the FM), nutrients, and DOC concentrations (in the SM) were assessed within months (SM) and stations (FM) using a one-way Kruskal-Wallis test for non-parametric analysis. Post hoc analysis was performed using Dunn's test (package: dunn.test (Dinno and Dinno 2017)) when necessary, following identification of significant differences (if Kruskal-Wallis test presented a p-value < 0.05). The same methodology was applied to examine differences in CO_2 fluxes, pCO_2, O_2%, and wind speed between day and night.

A Food Web (FW) type analysis was carried out using hierarchical agglomerative clustering (HAC), to analyze the biological parameters (HTTP, Chl*a*, and metazoans by size class), PP, and DOC at the SM. All parameters were converted to carbon biomass ($\mu gC\ L^{-1}$) to standardize and compare these different metrics (Table 1). For this analysis, Euclidean distance was used to measure the distances between groups, followed by to the Ward method (D1 or D2) as described in Masclaux et al. (2014). The analysis was performed using the following R packages: FactoMineR (Lê, Josse, and Husson 2008), factoexctra (Kassambara and Mundt 2017) cluster (Maechler 2018), ade4 (Thioulouse et al. 1997), and agricolae (De Mendiburu 2020).

To summarize and understand the relationships between PFWs, abiotic factors, and water carbon variables, a Principal Component Analysis (PCA) was performed (package: vegan (Dixon 2003)). This analysis was conducted only for the SM due to insufficient data for each station at the FM. Additionally, a Kendall Tau test was executed to examine the relationships between each parameter, as it is a robust and reliable estimator for small and non-normal samples (Xu et al. 2021).

3. Results

3.1. Temporal fluctuations in abiotic parameters

At the SM, average salinity and temperature values increased from 26.4 ± 0.1 and 11.5 ± 0.5°C in March to 34.3 ± 0.1 and 24.3 ± 1.2°C in July, respectively. DOC values were generally low but showed a slight increasing from 0.5 ± 0.0 mg L^{-1} in March to 3.6 ± 0.1 mg L^{-1} in August. Nutrient concentrations did not display a clear trend. NO_3^- and NH_4^+ reached their maximum concentrations in April (22.1 ± 1.4 μmol L^{-1} and 5.3 ± 1.9 μmol L^{-1}, respectively) and their minimum concentrations in June (0.0 μmol L^{-1} and 0.1 ± 0.1 μmol L^{-1}, respectively). NO_2^- concentrations also hit a low in June (0.2 ± 0.1 μmol L^{-1}), but peaked in

July (2.3 ± 1.4 µmol L^{-1}). PO$_4{}^{3-}$ concentrations increased steadily from 0.1 ± 0.0 µmol L^{-1} in March to 1.42 ± 0.0 µmol L^{-1} in August. Si varied from 33.7 ± 0.4 µmol L^{-1} in March to 45.5 ± 0.4 µmol L^{-1} in June. Turbidity showed no seasonal pattern, with the highest value of 34.4 ± 72.8 NTU recorded in August and the lowest value of 9.4 ± 2.6 NTU recorded in March.

At the FM, both salinity and temperature exhibited clear seasonal patterns. The highest values, which were notably high for a freshwater marsh, were recorded during summer at 8.0 ± 0.2 (TB) for salinity and 23.4 ± 2.0°C (TC) for temperature. In contrast, the lowest salinity and temperature values were observed during winter at 0.3 ± 0.0 (TA) and during autumn at 6.9 ± 0.8°C (TA), respectively. Turbidity was highest in summer at 178.2 ± 5.3 NTU (TA) and lowest in spring at 15.4 ± 5.6 NTU (TC). Nutrient concentrations did not follow a consistent pattern throughout the sampling period. Both NO$_3{}^-$ and NO$_2{}^-$ reached their peak concentrations in autumn, with NO$_3{}^-$ at 503.5 ± 10.6 µmol L^{-1} (TB) and NO$_2{}^-$ at 9.5 ± 1.2 µmol L^{-1} (TC). PO$_4{}^{3-}$ concentrations ranged from 0.02 to 0.9 µmol L^{-1}, except for site TC in winter, which saw a spike to 4.2 ± 4.0 µmol L^{-1}. Si showed its lowest value in winter at 15.0 ± 5.5 µmol L^{-1} and its highest in summer at 429.1 ± 19.3 µmol L^{-1} (TA). Finally, NH$_4{}^+$ levels varied from 0.4 ± 0.0 µmol L^{-1} in winter (TB) to 22.3 ± 1.3 µmol L^{-1} in spring (TA).

3.2. Variations in water pCO$_2$/O$_2$, wind speed, and water-air CO$_2$ fluxes

During the study period at the SM, water pCO$_2$ values consistently remained slightly oversaturated in comparison with the atmospheric equilibrium levels (417 ppmv), ranging between 541 ppmv during nighttime and 842 ppmv during the day (Fig. 3-A). Throughout this period, CO$_2$ fluxes were consistently positive, indicating a source for the atmosphere. Notably, both pCO$_2$ and NpCO$_2$ exhibited similar trends, while TpCO$_2$ deviated from this pattern (Fig. 3-A). Moreover, a seasonal pattern emerged, showing an inverse correlation between pCO$_2$ and O$_2$%, with May recording the highest pCO$_2$ levels (842 ± 81 ppmv) and the lowest O$_2$% (68.7 ± 1.7%) (Fig. 4-A, a, b). Conversely, CO$_2$ fluxes and wind speeds exhibited a synchronous trend, peaking in April (7.3 ± 2.9 mmol m^{-2} h^{-1}, 11.4 ± 0.4 m s^{-1}) and reaching their lowest in August (0.1 ± 0.0 mmol m^{-2} h^{-1}, 3.6 ± 1.0 m s^{-1}) (Fig. 4-A, c, d). Furthermore, significant day and night variations were observed for CO$_2$ fluxes, pCO$_2$, O$_2$%, and wind speeds (July and August only) (Kruskal-Wallis test, p-value < 0.05). Additionally, April stood out with significantly different CO$_2$ flux, pCO$_2$, and wind gust values compared to other months (Dunn's post hoc test, p-value < 0.05).

Seasonal variations in water pCO$_2$ were pronounced across all three stations at the FM, with TA exhibiting the most remarkable shift. During summer, TA displayed oversaturated pCO$_2$ levels (2595 ± 198 ppmv), contrasting with the remaining seasons where waters were undersaturated (252 ± 108 ppmv) (Fig. 3-B, a). Similar to observations at the SM, NpCO$_2$ values closely mirrored measured pCO$_2$, while TpCO$_2$ exhibited an inverse pattern. The most substantial discrepancy in CO$_2$ flux occurred during summer, with TB recording the highest value (5.5 ± 1.7 mmol m^{-2} h^{-1}) and TC the lowest (-3.7 ± 2.4 mmol m^{-2} h^{-1}) (Fig. 4-

B, c). Additionally, during summer, $O_2\%$ values at TA were slightly lower compared to the other two stations ($41.8 \pm 4.1\%$) (Fig. 4-B, b). At all three sites, significant differences were observed in pCO_2, $O_2\%$, CO_2 flux, and wind gust, with either positive (TA - TB, TA - TC) or negative (TB - TC) variations (Dunn's post hoc test, p-value < 0.05). Moreover, all four parameters showed significant differences between day and night (Kruskal-Wallis test, p-value < 0.05), except for CO_2 fluxes during spring, summer and winter at TA, and for all seasons at TC; and pCO_2 values in winter at station TB (Kruskal-Wallis test, p-value > 0.05).

3.3. Temporal dynamics in biotic parameters and planktonic food web analysis

In June, the SM exhibited its peak Chl$a$ biomass alongside Meso and HTTP abundances (Chl$a$: 10.37 µg L^{-1}, Meso: 1149.30 ind m^{-3}, HTTP: $7.48e^{05}$ cells mL^{-1}) (Fig. 4-A, e, f, g). Conversely, April marked the nadir for Chl$a$ biomass and Meso abundance (Chl$a$ = 0.12 µg L^{-1}, Meso = 225.35 ind m^{-3}), while HTTP hit its lowest count in July ($3.92e^{04}$ cells mL^{-1}). Monthly analysis revealed significant disparities in these biotic parameters (Kruskal-Wallis tests, p-value < 0.05). Notably, while Chl$a$ nano and pico fractions exhibited similar patterns without significant differences, Chl$a$ micro biomass was significantly smaller than nano and pico fractions (Dunn's post hoc test, p-value < 0.05). Although the highest PP rate occurred in June, no significant difference was observed (Fig. 4-A, h). Across the study period, smaller phytoplankton forms emerged as the most productive, exemplified by the nano fraction's peak PP value in June (77.45 ± 31.25 mg C $m^{-3} h^{-1}$), whereas Chl$a$ micro fraction consistently ranked lowest in PP production from March to August (Fig. 4-A, h).

At the FM, there were notable differences in seasonal variations of biotic parameters across stations. Particularly, TA exhibited higher Meso and Micro abundances (max Meso: 330.68 ind m^{-3} and Micro: 0.86 ind m^{-3}) compared to TB (max Meso: 10.37 ind m^{-3} and Micro: 0.90 ind m^{-3}) and TC (max Meso: 6.05 ind m^{-3} and Micro: 0.18 ind m^{-3}) (Fig. 4-B, e). However, Chl$a$ biomass did not follow the same trend, peaking in autumn at TB (Fig. 4-B, e, f). Both HTTP and Proto registered their lowest values at station TB (Fig. 4-B, g, h). While Chl$a$ micro was always significantly lower than the nano fractions at each station and season (Dunn's post hoc test, p-value < 0.05), exceptions were noted for TA in winter and TC in spring, summer and winter 2021 (Dunn's post hoc test, p-value > 0.05). Additionally, Meso, Micro, HTTP, and Proto abundances showed significant differences between stations and seasons (Dunn's post hoc tests, p-value < 0.05).

At the SM, HAC analysis revealed three distinct PFW topologies, labeled as FW1, FW2 and FW3 (Fig. 5-A, a). FW1, identified in June, emerged as a 'multivorous' FW, characterized by elevated carbon biomasses across all three fractions of Chl$a$, Meso, HTTP and DOC, alongside low nutrients concentrations (NO_3^-, NO_2^-, PO_4^{3-}, and NH_4^+) (Fig. 6). Within FW2, a temporal FW succession unveiled three distinct FWs, notably a 'weak herbivore' in March, April, and July, attributed to important nutrient levels, low Meso biomass, and relatively high microphytoplankton production (Fig. 5-A, b and 6). May revealed a 'microbial food web', possibly due to accumulating DOC resulting from Chl$a$ PP and Meso presence. Lastly, FW3

appeared as a 'weak multivorous' in August, characterized by high Chl*a* biomass across all size fractions, relatively lower heterotrophic biomasses (Meso and HTTP), and elevated nutrient concentrations.

In the FM, a large variability in PFWs was observed among stations, prompting separate HAC analyses for each. This approach uncovered distinct PFW types for each station, revealing nuanced variations within some (Fig. 5-B, a). Station TA exhibited two distinct 'multivorous' FWs: FW1.b, transitioning from a 'weak multivorous' state in spring to a 'multivorous' state in summer and autumn, characterized by fluctuating biomasses across all biotic variables alongside substantial nutrient concentrations, and FW2.b, categorized as 'multivorous (with low nutrients)' in winter, marked by higher biological biomasses but lower nutrient levels. At TB, FW3.b emerged as a 'biological winter' during spring, comprising predominantly predator biomasses alongside some nutrients. FW4.b displayed two distinct topologies: a 'weak multivorous' FW in summer, featuring elevated Chl*a* values and limited predator and HTTP presence alongside fluctuating nutrient concentrations, and a 'weak herbivorous' FW during autumn and winter (Fig. 5-B, a). Lastly, TC was divided into FW5.b, manifesting as a 'weak multivorous' FW in spring and winter alongside a 'biological winter', and FW6.b, characterized by a clear 'microbial FW' during summer and autumn (Fig. 5-B, a).

.

Figure 5 Clustering dendrograms for the HAC (hierarchical agglomerative clustering) applied to the biological matrix at (A, a) the L'Houmeau saltwater marsh (SM), with different food webs (FW1, FW2, FW3) defined by the cutting method "Ward.D1" (red line). Each number represents a replicate (1 to 3: March (FW2), 4 to 6: April (FW2), 7 to 9: May (FW2), 10 to 12: June (FW1), 13 to 15: July (FW2), 16 to 18: August (FW3); and (B, a) the Tasdon freshwater marsh (FM) stations (TA, TB, TC). There are two different food webs per station defined by the cutting method "Ward.D2" (red line). Each number represents a replicate (1 to 3: spring, 4 to 6 summer, 7 to 9: autumn, 10 to 12: winter), and colors indicate food web topology (FW1.b, FW2.b, FW3.b, FW4.b, FW5.b, FW6.b). Lastly, the association of food webs with either (A, b) monthly or (B, b) seasonal pCO$_2$ values is shown (A and B, b)

3.4. Relationships between water pCO$_2$ and planktonic food webs

At the SM, high daily mean water pCO$_2$ values (832 ppmv) were associated with the 'multivorous' FW type (Fig. 5-A, b and 6). Conversely, the 'weak multivorous' FW was related to the lowest pCO$_2$ values (averaging 638 ppmv over 24 hours). The relationship between pCO$_2$ and FW2 ('weak herbivore' and 'microbial food web') appeared less clear due to the high variability within this FW type (Fig. 5-A, b and 6). However, upon closer examination of FW2 nuances, associations could be discerned within each FW type individually. For instance, the 'weak herbivorous' FW type was mainly associated with lower pCO$_2$ values (ranging between 689 and 749 ppmv on average over 24 hours), while the 'microbial food web' manifested when pCO$_2$ values peaked (averaging 842 ppmv over 24 hours) (Fig. 5-A). Kendall correlation tests failed to reveal significant correlations between water pCO$_2$ and biotic parameters (Chl*a*, Meso, HTTP) (p-value

> 0.05). Conversely, negative correlations emerged between CO_2 fluxes and Meso and HTTP (p-value < 0.05; Kendall's tau = -0.46 and − 0.22, respectively). Chl$a$ exhibited negative correlation with O_2% (p-value < 0.05; Kendall's tau = -0.26) and positive correlation with PP (p-value < 0.05; Kendall's tau = 0.48). An inverse correlation was observed between Meso and O_2% (p-value < 0.05, Kendall's tau = -0.55). Lastly, pCO_2 showed positive correlation with DOC concentrations (p-value < 0.05; Kendall's tau = 0.41).

In the FM, comparing water pCO_2 values across stations revealed distinct patterns. The highest mean pCO_2 value (3020 ppmv) recorded at TA coincided with a 'multivorous' FW, while at TB, the highest mean pCO_2 values (1402 ppmv) were associated with a 'weak multivorous' FW, followed by a 'biological winter' (971 ppmv) (Fig. 5-B, b). At TC, both the highest and lowest pCO_2 values were linked to the 'microbial food web', with the second-largest pCO_2 value occurring alongside a 'biological winter' FW (Fig. 5-B). Kendall correlations for biotic and abiotic parameters did not reveal a consistent pattern within stations. At TA, both Meso and Micro exhibited positive relationships with pCO_2 (p-value > 0.05; Kendall's tau = 0.33 for both) and negative correlations with O_2 (p-value < 0.05; Kendall's tau = -0.33 for both). HTTP was negatively correlated with pCO_2, CO_2 fluxes, and O_2 (p-value < 0.05; Kendall's tau = 0.60, 0.30, and 0.30, respectively). At TB, inverse correlations were observed between CO_2 fluxes and both Chl$a$ and Meso (p-value < 0.05; Kendall's tau = -0.45 and − 0.33, respectively). Additionally, Micro exhibited negative relationships with both pCO_2 and O_2 (p-value < 0.05; Kendall's tau = -0.33 for both), while HTTP showed direct correlations with CO_2 flux and pCO_2 (p-value < 0.05; Kendall's tau = 0.30 and 0.60, respectively). Proto displayed a positive correlation with CO_2 flux but a negative correlation with O_2 (p-value < 0.05; Kendall's tau = 0.27 and − 0.58). Lastly, at TC, Chl$a$ and Proto were negatively correlated with O_2 (p-value < 0.05; Kendall's tau = -0.55 and − 0.79, respectively), while Meso and Micro exhibited inverse correlations with CO_2 fluxes and pCO_2 (p-value < 0.05; Kendall's tau = -0.33 for both). Similarly, HTTP showed negative relationships with O_2, CO_2 fluxes, and pCO_2 (p-value < 0.05; Kendall's tau = -0.60, -0.60, -0.30, respectively).

The PCA results facilitated the creation of a FW discrimination graphic at the monthly scale, utilizing both biotic and abiotic parameters (Fig. 7). The first two principal components (PC1 and PC2) explained 66.9% of the data variability, unveiling a seasonal gradient predominantly along the first component, with summer positioned at the left (reflecting maximal temperatures) and winter at the right. Principal components of PC1 included HTTP, Meso, Chl$a$, CO_2 flux, NO_3^-, and wind speed, while PC2 was primarily explained by PO_4 and turbidity. A conspicuous association emerged between elevated levels of Chl$a$, Meso, and HTTP with high pCO_2 and PP. Moreover, all biotic factors, alongside pCO_2 values, were related to FW1, representative of June (Fig. 3-A and 6). Simultaneously, this seasonal gradient indicated a decline in O_2% saturation and CO_2 flux for that particular month. The variability within FW2 revealed a negative association with turbidity and PO_4 in March, but a positive relationship with CO_2 flux and O_2% in April, with pCO_2 in May, and with turbidity and PO_4 in July. Lastly, FW3 was also associated with both turbidity and PO_4 values (Fig. 7).

4. Discussion

4.1. Marsh typologies as carbon sinks around the globe

"Blue Carbon" ecosystems are not only important from an ecological point of view, but also crucial for the economy and society due to their role as regulatory systems. Their importance stems from their ability to mitigate flooding risks, improve water quality, enhance biodiversity, and store large amounts of carbon in their soils and biomass (C. M. Duarte, Middelburg, and Caraco 2005; Carlos M. Duarte et al. 2013; Mcleod et al. 2011; Monnoyer-Smith 2019). Both saltwater and freshwater marshes can act as important atmospheric CO_2 sinks (Guo et al. 2010; Kostyrka 2021; Mayen et al. 2024; Schäfer et al. 2014) or sources (Kayranli et al. 2010), depending on spatial (water bodies, habitats, biological/sedimentary stocks, management) and temporal (diurnal, tidal, seasonal, (inter-annual) scales. Furthermore, studies by Artigas et al. (2015), Miller and Fujii (2011), Schäfer et al. (2014) and Tuittila et al. (1999) highlighted that wetland restoration can transform marshes, deltas, or peatlands from atmospheric CO_2 sources to sinks. Conversely, Jimenez et al. (2012) observed that anthropogenic disruption (e.g., human-driven hydrologic changes) caused a freshwater marsh to shift from a strong CO_2 sink to a light CO_2 source.

In the present study, at the FM, lower CO_2 emissions were measured post-restoration Mayen (2024), with some periods even exhibiting CO_2 sink behavior, depending on the station and season. For instance, at station TC, with the input of saltwater during the summer of 2021, CO_2 flux was recorded at -3.70 ± 2.37 mmol m^{-2} h^{-1}. In contrast, the SM remained a CO_2 source throughout the study period (from March to August; Fig. 3-A and 4-A, a, c). This finding contradicts previous research indicating that saltwater environments typically act as CO_2 sinks (Mayen et al. 2023), as well as *in situ* measurements from wetlands along a land-sea continuum in the La Rochelle metropolitan area (Polsenaere et al., unpublished results). This discrepancy may be due to the closed structure of the SM, which differs from the more commonly studied open saltwater marshes (Alongi 2020; Mayen et al. 2023; Thorhaug et al. 2019). Another possible explanation is that the low vegetation density and reduced photosynthetic activity in the SM result in higher respiration rates remained than primary production. This is supported by the O_2% values, which were inversely related to pCO_2 values, likely indicating low phytoplankton production and higher respiration rates.

As mentioned earlier, from March until August 2021, the SM remained a weak atmospheric carbon source characterized by periods of water CO_2 oversaturation with pCO_2 variations between 600 and 900 ppmv. In our study, both temperature ($TpCO_2$) and non-temperature ($NtpCO_2$) effects predominantly influenced water pCO_2 at both the SM and the FM, though $NpCO_2$ appeared to have a greater impact on the measured pCO_2 levels (Fig. 3-A, B). For instance, at the SM, the $\Delta TpCO_2$ was smaller than $\Delta NpCO_2$ (465 ppmv versus 682 ppmv, respectively) throughout the entire study period. A similar pattern was observed at the FM between spring and autumn 2021. $\Delta TpCO_2$ and $\Delta NpCO_2$ were: at TA 2831 ppmv (ranging from 287 to 3118 ppmv) and 3446 ppmv (ranging from 216 to 3662 ppmv) respectively; at TB $\Delta TpCO_2$ was 1338 ppmv (ranging from 119 to 1457 ppmv) and $\Delta NpCO_2$ 3467 ppmv (ranging from 100 to 3567 ppmv);

and at TC, they were 987 ppmv (ranging from 251 to 1238 ppmv) and 1680 ppmv (ranging from 100 to 1780 ppmv) respectively. The effects of $NpCO_2$ on pCO_2 can be linked to environmental factors such as salinity and DOC, indicating advection processes, and biotic factors, including photosynthesis and microbial respiration processes, that occurred at the SM. This result is comparable to Mayen et al. (2023), who showed that horizontal advection processes (upstream and downstream) significantly influence on water pCO_2 dynamics in salt marshes (salt ponds) near the Fier d'Ars (Île de Ré, France).

In this study, many factors could have influenced the observed changes in CO_2 behavior. These include temperature and particularly non-temperature effects (Fig. 3-B), replanted vegetation (63,000 aquatic plants), and nutrient concentration along with salinity variations. These factors induced important changes, such as increases in Chl*a* phytoplankton biomass and shifts in FW topology. Biotic parameters were also crucial in controlling pCO_2 at the SM, as indicated by O_2% values inversely related to pCO_2 values from March to August 2021, likely reflecting low phytoplankton production and higher respiration rates. Conversely, the FM shifted from being strong water CO_2 source to exhibiting a balanced behavior as both a weak source and a sink, depending on the seasons and stations (Fig. 4-B, a, c).

4.2. Food web topologies and their relationship with water pCO_2 at studied marshes

Although no significant correlation between water pCO_2 and biotic factors was found at the SM, relationships between pCO_2 and PFW were clearly established during our study. Three different FW topologies were identified, each with nuances: a 'multivorous' FW in June (FW1) and a 'microbial food web' in May (FW2) exhibited mean high pCO_2 values (832 ppmv and 842 ppmv, respectively), while a 'weak multivorous' FW was associated with a lower mean pCO_2 value (638 ppmv) during August (FW3). Additionally, a 'weak herbivorous' FW occurred in March, April and July (FW2), with variable mean pCO_2 values ranging between 689 and 749 ppmv. These FW topologies have been previously described by Legendre and Rassoulzadegan (1995), Masclaux et al. (2014) and Tortajada (2011). Legendre and Rassoulzadegan (1995) noted that some PFWs, such as 'multivorous' and 'microbial food web' FWs, were more stable over time compared to others, like the 'herbivorous' FW. At the SM, the two stable FWs ('multivorous' and 'microbial food web') were associated with high mean pCO_2 values (832 and 842 ppmv, respectively). This could be attributed to the high abundance of Meso and HTTP and the weak PP for the multivorous FW, or to the increased concentration of DOC in May for the 'microbial food web'. Prairie, Bird, and Cole (2002) and Lapierre et al. (2013) have shown that DOC increases can directly raise water pCO_2. Conversely, the transitory FWs ('weak herbivorous' and 'weak multivorous') were associated with medium or low mean pCO_2 values (Fig. 6). These findings suggest that pCO_2 tends to accumulate more during stable FW occurrences than during transient ones.

At the FM, the absence of clear seasonality in FW types observed throughout 2021 could be attributed to the recent restoration process initiated in 2019, which may have disrupted the marsh's return to an equilibrium state by 2021. Therefore, further monitoring of both carbon dynamics and FW topologies is

necessary to clarify this absence of seasonality. Nevertheless, specific FW occurrences were notable during the study period. The 'biological winter' FW identified in spring 2021 at station TB (FW3.b) and in winter at station TC (FW5.b) were both associated with elevated pCO_2 values (971 and 959 ppmv, respectively). In contrast, the 'weak herbivorous' FW observed from autumn to winter at TB (FW4.b) was linked to the lowest pCO_2 values (127 and 299 ppmv, respectively). At station TA, extreme pCO_2 values (298 and 3020 ppmv in autumn and summer, respectively) were attributed to the 'multivorous' FW (FW2.b). This association could be explained by lower Chl*a* nano and pico biomasses along with higher HTTP and Meso biomasses measured in summer compared to autumn. A similar pattern was observed for the 'microbial food web' identified at TC (FW6.b), which was associated with very high Chl*a* biomasses measured during summer. Conversely, no clear relationship was found between the 'weak multivorous' FWs and pCO_2 values, likely due to the lack of biological equilibrium.

4.3. Conclusions

This comparative analysis of two distinct marsh FW topologies allowed us to discern both similarities and differences between sites regarding carbon and FW relationships. Despite their typological disparities, both the SM and the FM functioned as CO_2 sources, with the FM exhibiting a weaker source tendency and occasionally acting as a carbon sink. Despite the divergent marsh characteristics (including contrasting salinity values, nutrient concentrations, and water regulation/management), our original approach clearly highlighted five food web topologies and their associated pCO_2 values (Fig. 8). These included three stable types ('biological winter', 'microbial food web', 'multivorous' food webs) with high pCO_2 values at both sites, as well as two transient types ('weak multivorous' and 'weak herbivorous') with lower and more variable pCO_2 values (Fig. 8). While four of these food webs had been previously described in literature (Legendre and Rassoulzadegan 1995; Masclaux et al. 2014; Tortajada 2011), two known PFW types, namely 'herbivorous' and 'microbial loop', were not observed in our study. Additionally, the 'biological winter' FW was not identified at the SM.

As the first registered study investigating the link between plankton FWs and water carbon in marshes, there is certainly room for improvement. One possible upgrade would be to adjust the sampling frequency, either by conducting monthly or seasonal sampling, and/or extending the duration of the study (over several years). Additionally, incorporating measurements of respiration rate could provide valuable insights into carbon dynamics within the ecosystem. Further research is encouraged to enhance our understanding of the relationship between PFW and water pCO_2.

Declarations

Competing interests

The authors declare that they have no known competing or financial interests or personal relationships that could have appeared to influence the work reported in this paper.

Contribution

The study was conceptualized by C.D. and P.Po. . J.M., R.M. and L.B. contributed with formal analysis. F-X.R., P.Pi., C.E. and B.D. contributed to the methodology and data sampling and curation. M.V. helped with founding and editing. L.X. has done the data analysis, visualization, and writing of the original draft. Reviewing and editing the manuscript was done by L.X., C.D.and P.Po.. L.X., R.M., J.M., L.B., B.D., P.Pi., C.E., M.V., F-X.R., F.A., M.T., C.D., P.Po. contributed to later versions of the manuscript. All authors read and approved the final manuscript.

Ethics declaration

The authors declare that they have no conflict of interest. This study does not involve human participants.

Data Availability Statement

Data will be made available on request.

References

1. Adamczyk, Emily M., and Jonathan B. Shurin. 2015. "Seasonal Changes in Plankton Food Web Structure and Carbon Dioxide Flux from Southern California Reservoirs." PLOS ONE 10(10): e0140464. doi:10.1371/journal.pone.0140464.
2. Afonso, Marine. 2023. "Analyse Des Typologies et Surfaces Des Milieux Carbone Bleu de l'Agglomération de La Rochelle. Rapport Final."
3. Alongi, Daniel M. 2020. "Carbon Balance in Salt Marsh and Mangrove Ecosystems: A Global Synthesis." Journal of Marine Science and Engineering 8(10): 767. doi:10.3390/jmse8100767.
4. Amann, B., E. Chaumillon, S. Schmidt, L. Olivier, J. Jupin, M. C. Perello, and J. P. Walsh. 2023. "Multi-Annual and Multi-Decadal Evolution of Sediment Accretion in a Saltmarsh of the French Atlantic Coast: Implications for Carbon Sequestration." Estuarine, Coastal and Shelf Science 293: 108467. doi:10.1016/j.ecss.2023.108467.
5. Aminot, Alain, and R Kerouel. 2007. "Dosage Automatique Des Nutriments Dans Les Eaux Marines. Ed. Quae, Ifremer. 188p."

6. Aminot, Alain, and Roger Kérouel. 2004. *Hydrologie des écosystèmes marins: paramètres et analyses*. Editions Quae.

7. Artigas, Francisco, Jin Young Shin, Christine Hobble, Alejandro Marti-Donati, Karina V. R. Schäfer, and Ildiko Pechmann. 2015. "Long Term Carbon Storage Potential and CO2 Sink Strength of a Restored Salt Marsh in New Jersey." Agricultural and Forest Meteorology 200: 313–21. doi:10.1016/j.agrformet.2014.09.012.

8. Azim, M. E., Marc C. J. Verdegem, Anne A. van Dam, and Malcolm C. M. Beveridge. 2005. *Periphyton: Ecology, Exploitation and Management*. CABI.

9. Beaugrand, Grégory. 2005. "Monitoring Pelagic Ecosystems Using Plankton Indicators." ICES Journal of Marine Science 62(3): 333–38. doi:10.1016/j.icesjms.2005.01.002.

10. Berg, Peter, Marie Lise Delgard, Pierre Polsenaere, Karen J. McGlathery, Scott C. Doney, and Amelie C. Berger. 2019. "Dynamics of Benthic Metabolism, O2, and pCO2 in a Temperate Seagrass Meadow." Limnology and Oceanography 64(6): 2586–2604. doi:10.1002/lno.11236.

11. Bergeon, Lauriane, Frédéric Azémar, Claire Carré, Bénédicte Dubillot, Claire Emery, Hélène Agogué, Philippe Pineau, et al. 2023. "Distribution and Trophic Functioning of Planktonic Communities in Coastal Marshes in Atlantic Coast of France." Estuarine, Coastal and Shelf Science 291: 108430. doi:10.1016/j.ecss.2023.108430.

12. Buskey, Edward J., and Cammie J. Hyatt. 2006. "Use of the FlowCAM for Semi-Automated Recognition and Enumeration of Red Tide Cells (*Karenia Brevis*) in Natural Plankton Samples." Harmful Algae 5(6): 685–92. doi:10.1016/j.hal.2006.02.003.

13. Canadell, Josep G., Pedro M.S. Monteiro, Marcos H. Costa, Leticia Cotrim Da Cunha, Peter M. Cox, Alexey V. Eliseev, Stephanie Henson, et al. 2021. "Global Carbon and Other Biogeochemical Cycles and Feedbacks." In *IPCC AR6 WGI, Final Government Distribution*,, Chap. 5. https://hal.science/hal-03336145 (May 7, 2024).

14. Chmura, Gail L., Shimon C. Anisfeld, Donald R. Cahoon, and James C. Lynch. 2003. "Global Carbon Sequestration in Tidal, Saline Wetland Soils." Global Biogeochemical Cycles 17(4). doi:10.1029/2002GB001917.

15. Dai, Minhan, Zhongming Lu, Weidong Zhai, Baoshan Chen, Zhimian Cao, Kuanbo Zhou, Wei-Jun Cai, and Chen-Tung Arthur Chenc. 2009. "Diurnal Variations of Surface Seawater pCO2 in Contrasting Coastal Environments." Limnology and Oceanography 54(3): 735–45. doi:10.4319/lo.2009.54.3.0735.

16. De Mendiburu, F. 2020. "AGRICOLAE: Statistical Procedures for Agricultural Research, Version 1.2-4."

17. Del Giorgio, Paul A., Jonathan J. Cole, and André Cimbleris. 1997. "Respiration Rates in Bacteria Exceed Phytoplankton Production in Unproductive Aquatic Systems." Nature 385(6612): 148–51. doi:10.1038/385148a0.

18. Del Giorgio, Paul A., and Peter Williams. 2005. *Respiration in Aquatic Ecosystems*. OUP Oxford.

19. Dinno, A, and M Dinno. 2017. "Package 'Dunn. Test'. CRAN Repos, 10, 1–7."

20. Dixon, Philip. 2003. "VEGAN, a Package of R Functions for Community Ecology." Journal of Vegetation Science 14(6): 927–30. doi:10.1111/j.1654-1103.2003.tb02228.x.

21. Duarte, C. M., J. J. Middelburg, and N. Caraco. 2005. "Major Role of Marine Vegetation on the Oceanic Carbon Cycle." Biogeosciences 2(1): 1–8. doi:10.5194/bg-2-1-2005.

22. Duarte, Carlos M., Iñigo J. Losada, Iris E. Hendriks, Inés Mazarrasa, and Núria Marbà. 2013. "The Role of Coastal Plant Communities for Climate Change Mitigation and Adaptation." Nature Climate Change 3(11): 961–68. doi:10.1038/nclimate1970.

23. Dumont, Henri J., Isabella Van de Velde, and Simonne Dumont. 1975. "The Dry Weight Estimate of Biomass in a Selection of Cladocera, Copepoda and Rotifera from the Plankton, Periphyton and Benthos of Continental Waters." Oecologia 19(1): 75–97. doi:10.1007/BF00377592.

24. Fagherazzi, Sergio, Patricia L. Wiberg, Stijn Temmerman, Eric Struyf, Yong Zhao, and Peter A. Raymond. 2013. "Fluxes of Water, Sediments, and Biogeochemical Compounds in Salt Marshes." Ecological Processes 2(1): 3. doi:10.1186/2192-1709-2-3.

25. Fournier, Jonathan, Emmanuelle Levesque, Stephane Pouvreau, Marcel Le Pennec, and Gilles Le Moullac. 2012. "Influence of Plankton Concentration on Gametogenesis and Spawning of the Black Lip Pearl Oyster *Pinctada Margaritifera* in Ahe Atoll Lagoon (Tuamotu Archipelago, French Polynesia)." Marine Pollution Bulletin 65(10): 463–70. doi:10.1016/j.marpolbul.2012.03.027.

26. Friedlingstein, Pierre, Michael O'Sullivan, Matthew W. Jones, Robbie M. Andrew, Luke Gregor, Judith Hauck, Corinne Le Quéré, et al. 2022. "Global Carbon Budget 2022." Earth System Science Data 14(11): 4811–4900. doi:10.5194/essd-14-4811-2022.

27. Greiner, Jill T., Karen J. McGlathery, John Gunnell, and Brent A. McKee. 2013. "Seagrass Restoration Enhances 'Blue Carbon' Sequestration in Coastal Waters." PLOS ONE 8(8): e72469. doi:10.1371/journal.pone.0072469.

28. Gundersen, Kjell, Mikal Heldal, Svein Norland, Duncan A. Purdie, and Anthony H. Knap. 2002. "Elemental C, N, and P Cell Content of Individual Bacteria Collected at the Bermuda Atlantic Time-Series Study (BATS) Site." Limnology and Oceanography 47(5): 1525–30. doi:10.4319/lo.2002.47.5.1525.

29. Guo, Zhaodi, Jingyun Fang, Yude Pan, and Richard Birdsey. 2010. "Inventory-Based Estimates of Forest Biomass Carbon Stocks in China: A Comparison of Three Methods." Forest Ecology and Management 259(7): 1225–31. doi:10.1016/j.foreco.2009.09.047.

30. Jähne, B, G Heinz, and W Dietrich. 1987. "Measurement of the Diffusion Coefficients of Sparingly Soluble Gases in Water. Journal of Geophysical Research: Oceans, 92(C10), 10767–10776."

31. Jimenez, K. L., G. Starr, C. L. Staudhammer, J. L. Schedlbauer, H. W. Loescher, S. L. Malone, and S. F. Oberbauer. 2012. "Carbon Dioxide Exchange Rates from Short- and Long-Hydroperiod Everglades Freshwater Marsh." Journal of Geophysical Research: Biogeosciences 117(G4). doi:10.1029/2012JG002117.

32. Kassambara, Alboukadel. 2019. "Practical Statistics in R II - Comparing Groups: Numerical Variables."

33. Kassambara, Alboukadel, and F Mundt. 2017. "Package 'Factoextra'. Extract and Visualize the Results of Multivariate Data Analyses, 76(2)."

34. Kayranli, Birol, Miklas Scholz, Atif Mustafa, and Åsa Hedmark. 2010. "Carbon Storage and Fluxes within Freshwater Wetlands: A Critical Review." Wetlands 30(1): 111–24. doi:10.1007/s13157-009-0003-4.

35. Kostyrka, P. 2021. "Dynamique Des Échanges de CO2 Atmosphérique Mesurés Par Covariance Des Turbulences et Facteurs de Contrôle Associés Dans Un Marais Salé Tempéré. Thèse de Master."

36. Lapierre, Jean-François, François Guillemette, Martin Berggren, and Paul A. del Giorgio. 2013. "Increases in Terrestrially Derived Carbon Stimulate Organic Carbon Processing and CO2 Emissions in Boreal Aquatic Ecosystems." Nature Communications 4(1): 2972. doi:10.1038/ncomms3972.

37. Lê, Sébastien, Julie Josse, and François Husson. 2008. "FactoMineR: An R Package for Multivariate Analysis." Journal of Statistical Software 25: 1–18. doi:10.18637/jss.v025.i01.

38. Legendre, Louis, and Fereidoun Rassoulzadegan. 1995. "Plankton and Nutrient Dynamics in Marine Waters." Ophelia 41(1): 153–72. doi:10.1080/00785236.1995.10422042.

39. Legendre, Louis, and Richard B. Rivkin. 2005. "Integrating Functional Diversity, Food Web Processes, and Biogeochemical Carbon Fluxes into a Conceptual Approach for Modeling the Upper Ocean in a High-CO2 World." Journal of Geophysical Research: Oceans 110(C9). doi:10.1029/2004JC002530.

40. Macreadie, Peter I, Daniel A Nielsen, Jeffrey J Kelleway, Trisha B Atwood, Justin R Seymour, Katherina Petrou, Rod M Connolly, et al. 2017. "Can We Manage Coastal Ecosystems to Sequester More Blue Carbon?" Frontiers in Ecology and the Environment 15(4): 206–13. doi:10.1002/fee.1484.

41. Macreadie, Peter I., Oscar Serrano, Damien T. Maher, Carlos M. Duarte, and John Beardall. 2017. "Addressing Calcium Carbonate Cycling in Blue Carbon Accounting." Limnology and Oceanography Letters 2(6): 195–201. doi:10.1002/lol2.10052.

42. Maechler, M. 2018. "Cluster: Cluster Analysis Basics and Extensions. R Package Version 2.0. 7–1."

43. Marie, Dominique, Frédéric Partensky, Daniel Vaulot, and Corina Brussaard. 1999. "Enumeration of Phytoplankton, Bacteria, and Viruses in Marine Samples." Current Protocols in Cytometry 10(1): 11.11.1-11.11.15. doi:10.1002/0471142956.cy1111s10.

44. Marquis, E., N. Niquil, D. Delmas, H. J. Hartmann, D. Bonnet, F. Carlotti, A. Herbland, et al. 2007. "Inverse Analysis of the Planktonic Food Web Dynamics Related to Phytoplankton Bloom Development on the Continental Shelf of the Bay of Biscay, French Coast." Estuarine, Coastal and Shelf Science 73(1): 223–35. doi:10.1016/j.ecss.2007.01.003.

45. Masclaux, Hélène, Sébastien Tortajada, Olivier Philippine, François-Xavier Robin, and Christine Dupuy. 2014. "Planktonic Food Web Structure and Dynamic in Freshwater Marshes after a Lock Closing in Early Spring." Aquatic Sciences 77(1): 115–28. doi:10.1007/s00027-014-0376-1.

46. Mayen, Jérémy. 2024. "Échanges de CO2 Atmosphérique Dans Les Marais Charentais: Processus, Dynamique et Facteurs de Contrôle Associés. Thèse de Doctorat En Écologie et Biologie Marine. Nantes Université."

47. Mayen, Jérémy, Pierre Polsenaere, Éric Lamaud, Marie Arnaud, Pierre Kostyrka, Jean-Marc Bonnefond, Philippe Geairon, et al. 2024. "Atmospheric CO_2 Exchanges Measured by Eddy Covariance

over a Temperate Salt Marsh and Influence of Environmental Controlling Factors." Biogeosciences 21(4): 993–1016. doi:10.5194/bg-21-993-2024.

48. Mayen, Jérémy, Pierre Polsenaere, Aurore Regaudie de Gioux, Christine Dupuy, Marie Vagner, Jean-Christophe Lemesle, Benoit Poitevin, and Philippe Souchu. 2023. "Influence of Typology and Management Practices on Water pCO2 and Atmospheric CO2 Fluxes over Two Temperate Shelf–Estuary–Marsh Water Continuums." Regional Studies in Marine Science 67: 103209. doi:10.1016/j.rsma.2023.103209.

49. Mcleod, Elizabeth, Gail L Chmura, Steven Bouillon, Rodney Salm, Mats Björk, Carlos M Duarte, Catherine E Lovelock, William H Schlesinger, and Brian R Silliman. 2011. "A Blueprint for Blue Carbon: Toward an Improved Understanding of the Role of Vegetated Coastal Habitats in Sequestering CO2." Frontiers in Ecology and the Environment 9(10): 552–60. doi:10.1890/110004.

50. Miller, Robin, and R. Fujii. 2011. "Re-Establishing Marshes Can Turn a Current Carbon Source into a Carbon Sink in the Sacramento-San Joaquin Delta of California, USA." River Deltas: Types, Structures and Ecology: 1–34.

51. Moncelon, Raphaël. 2022. "Couplage benthos-pelagos en marais littoraux de Charente-Maritime: contribution du compartiment sédimentaire à la capacité épuratrice des eaux de surface." phdthesis. Université de La Rochelle. https://theses.hal.science/tel-04030000 (February 14, 2024).

52. Moncelon, Raphaël, Edouard Metzger, Philippe Pineau, Claire Emery, Eric Bénéteau, Charlotte de Lignières, Olivier Philippine, François-Xavier Robin, and Christine Dupuy. 2022. "Drivers for Primary Producers' Dynamics: New Insights on Annual Benthos Pelagos Monitoring in Anthropised Freshwater Marshes (Charente-Maritime, France)." Water Research 221: 118718. doi:10.1016/j.watres.2022.118718.

53. Monnoyer-Smith, L. 2019. "La Séquestration de Carbone Par Les Écosystèmes En France. Commissariat Général Du Développement Durable."

54. Moreau, Sébastien, Eugenia di Fiori, Irene R. Schloss, Gastón O. Almandoz, José L. Esteves, Flavio E. Paparazzo, and Gustavo A. Ferreyra. 2013. "The Role of Phytoplankton Composition and Microbial Community Metabolism in Sea–Air ΔpCO2 Variation in the Weddell Sea." Deep Sea Research Part I: Oceanographic Research Papers 82: 44–59. doi:10.1016/j.dsr.2013.07.010.

55. Nielsen, E. Steemann. 1951. "Measurement of the Production of Organic Matter in the Sea by Means of Carbon-14." Nature 167(4252): 684–85. doi:10.1038/167684b0.

56. Niquil, Nathalie, Gretta Bartoli, Jotaro Urabe, George A. Jackson, Louis Legendre, Christine Dupuy, and M. Kumagai. 2006. "Carbon Steady-State Model of the Planktonic Food Web of Lake Biwa, Japan." Freshwater Biology 51(8): 1570–85. doi:10.1111/j.1365-2427.2006.01595.x.

57. Nyman, John A. 2011. "Ecological Functions of Wetlands." In *Wetlands: Integrating Multidisciplinary Concepts*, ed. Ben A. LePage. Dordrecht: Springer Netherlands, 115–28. doi:10.1007/978-94-007-0551-7_6.

58. Polsenaere, Pierre, Jonathan Deborde, Guillaume Detandt, Luciana O. Vidal, Marcela A. P. Pérez, Vincent Marieu, and Gwenaël Abril. 2013. "Thermal Enhancement of Gas Transfer Velocity of CO2 in

an Amazon Floodplain Lake Revealed by Eddy Covariance Measurements." Geophysical Research Letters 40(9): 1734–40. doi:10.1002/grl.50291.

59. Polsenaere, Pierre, Bruno Delille, Dominique Poirier, Céline Charbonnier, Jonathan Deborde, Aurélia Mouret, and Gwenaël Abril. 2023. "Seasonal, Diurnal, and Tidal Variations of Dissolved Inorganic Carbon and pCO2 in Surface Waters of a Temperate Coastal Lagoon (Arcachon, SW France)." Estuaries and Coasts 46(1): 128–48. doi:10.1007/s12237-022-01121-6.

60. Prairie, Yves T., David F. Bird, and Jonathan J. Cole. 2002. "The Summer Metabolic Balance in the Epilimnion of Southeastern Quebec Lakes." Limnology and Oceanography 47(1): 316–21. doi:10.4319/lo.2002.47.1.0316.

61. Putt, Mary, and Diane K. Stoecker. 1989. "An Experimentally Determined Carbon: Volume Ratio for Marine 'Oligotrichous' Ciliates from Estuarine and Coastal Waters." Limnology and Oceanography 34(6): 1097–1103. doi:10.4319/lo.1989.34.6.1097.

62. Raymond, Peter A., and J. J. Cole. 2001. "Gas Exchange in Rivers and Estuaries: Choosing a Gas Transfer Velocity. Estuaries 24, 312. Https://Doi.Org/10.2307/1352954."

63. Ribas-Ribas, Mariana, Abelardo Gómez-Parra, and Jesús M. Forja. 2011. "Air–Sea CO2 Fluxes in the North-Eastern Shelf of the Gulf of Cádiz (Southwest Iberian Peninsula)." Marine Chemistry 123(1): 56–66. doi:10.1016/j.marchem.2010.09.005.

64. Schäfer, K. V. R., R. Tripathee, F. Artigas, T. H. Morin, and G. Bohrer. 2014. "Carbon Dioxide Fluxes of an Urban Tidal Marsh in the Hudson-Raritan Estuary." Journal of Geophysical Research: Biogeosciences 119(11): 2065–81. doi:10.1002/2014JG002703.

65. Shiomoto, Akihiro. 1997. "Size-Fractionated Chlorophyll a Concentration and Primary Production in the Okhotsk Sea in October and November 1993, with Special Reference to the Influence of Dichothermal Water."

66. Sieburth, John McN., Victor Smetacek, and Jürgen Lenz. 1978. "Pelagic Ecosystem Structure: Heterotrophic Compartments of the Plankton and Their Relationship to Plankton Size Fractions 1." Limnology and Oceanography 23(6): 1256–63. doi:10.4319/lo.1978.23.6.1256.

67. Sobek, S, Tranvik L. J., and J. J. Cole. 2005. "Temperature Independence of Carbon Dioxide Supersaturation in Global Lakes - Global Biogeochemical Cycles - Wiley Online Library." https://agupubs.onlinelibrary.wiley.com/doi/full/10.1029/2004GB002264 (April 25, 2024).

68. Takahashi, Taro, Richard A. Feely, Ray F. Weiss, Rik H. Wanninkhof, David W. Chipman, Stewart C. Sutherland, and Timothy T. Takahashi. 1997. "Global Air-Sea Flux of CO2: An Estimate Based on Measurements of Sea–Air pCO2 Difference." *Proceedings of the National Academy of Sciences* 94(16): 8292–99. doi:10.1073/pnas.94.16.8292.

69. Takahashi, Taro, Stewart C. Sutherland, Colm Sweeney, Alain Poisson, Nicolas Metzl, Bronte Tilbrook, Nicolas Bates, et al. 2002. "Global Sea–Air CO2 Flux Based on Climatological Surface Ocean *p*CO2, and Seasonal Biological and Temperature Effects." Deep Sea Research Part II: Topical Studies in Oceanography 49(9): 1601–22. doi:10.1016/S0967-0645(02)00003-6.

70. Thioulouse, Jean, Daniel Chessel, Sylvain Dole´dec, and Jean-Michel Olivier. 1997. "ADE-4: A Multivariate Analysis and Graphical Display Software." Statistics and Computing 7(1): 75–83. doi:10.1023/A:1018513530268.

71. Thorhaug, Anitra L., Helen M. Poulos, Jorge López-Portillo, Jordan Barr, Ana Laura Lara-Domínguez, Tim C. Ku, and Graeme P. Berlyn. 2019. "Gulf of Mexico Estuarine Blue Carbon Stock, Extent and Flux: Mangroves, Marshes, and Seagrasses: A North American Hotspot." *Science of The Total Environment* 653: 1253–61. doi:10.1016/j.scitotenv.2018.10.011.

72. Tilzer, Max M., and Zvy Dubinsky. 1987. "Effects of Temperature and Day Length on the Mass Balance of Antarctic Phytoplankton." Polar Biology 7(1): 35–42. doi:10.1007/BF00286822.

73. Tortajada, Sébastien. 2011. "De l'étude du fonctionnement des réseaux trophiques planctoniques des marais de Charente Maritime vers la recherche d'indicateurs." phdthesis. Université de La Rochelle. https://theses.hal.science/tel-00808599 (May 7, 2024).

74. Tuittila, Eeva-Stiina, Veli-Matti Komulainen, Harri Vasander, and Jukka Laine. 1999. "Restored Cut-Away Peatland as a Sink for Atmospheric CO2." Oecologia 120(4): 563–74. doi:10.1007/s004420050891.

75. Verhoeven, Jos T. A., Berit Arheimer, Chengqing Yin, and Mariet M. Hefting. 2006. "Regional and Global Concerns over Wetlands and Water Quality." Trends in Ecology & Evolution 21(2): 96–103. doi:10.1016/j.tree.2005.11.015.

76. Vincent, Dorothée, Christophe Luczak, and Benoît Sautour. 2002. "Effects of a Brief Climatic Event on Zooplankton Community Structure and Distribution in Arcachon Bay (France)." Journal of the Marine Biological Association of the United Kingdom 82(1): 21–30. doi:10.1017/S0025315402005143.

77. Xu, S, M Chen, T Feng, L Zhan, L Zhou, and G Yu. 2021. "Use Ggbreak to Effectively Utilize Plotting Space to Deal with Large Datasets and Outliers. Frontiers in Genetics, 12, 2122."

78. Yentsch, Charles S, and David W Menzel. 1963. "A Method for the Determination of Phytoplankton Chlorophyll and Phaeophytin by Fluorescence." Deep Sea Research and Oceanographic Abstracts 10(3): 221–31. doi:10.1016/0011-7471(63)90358-9.
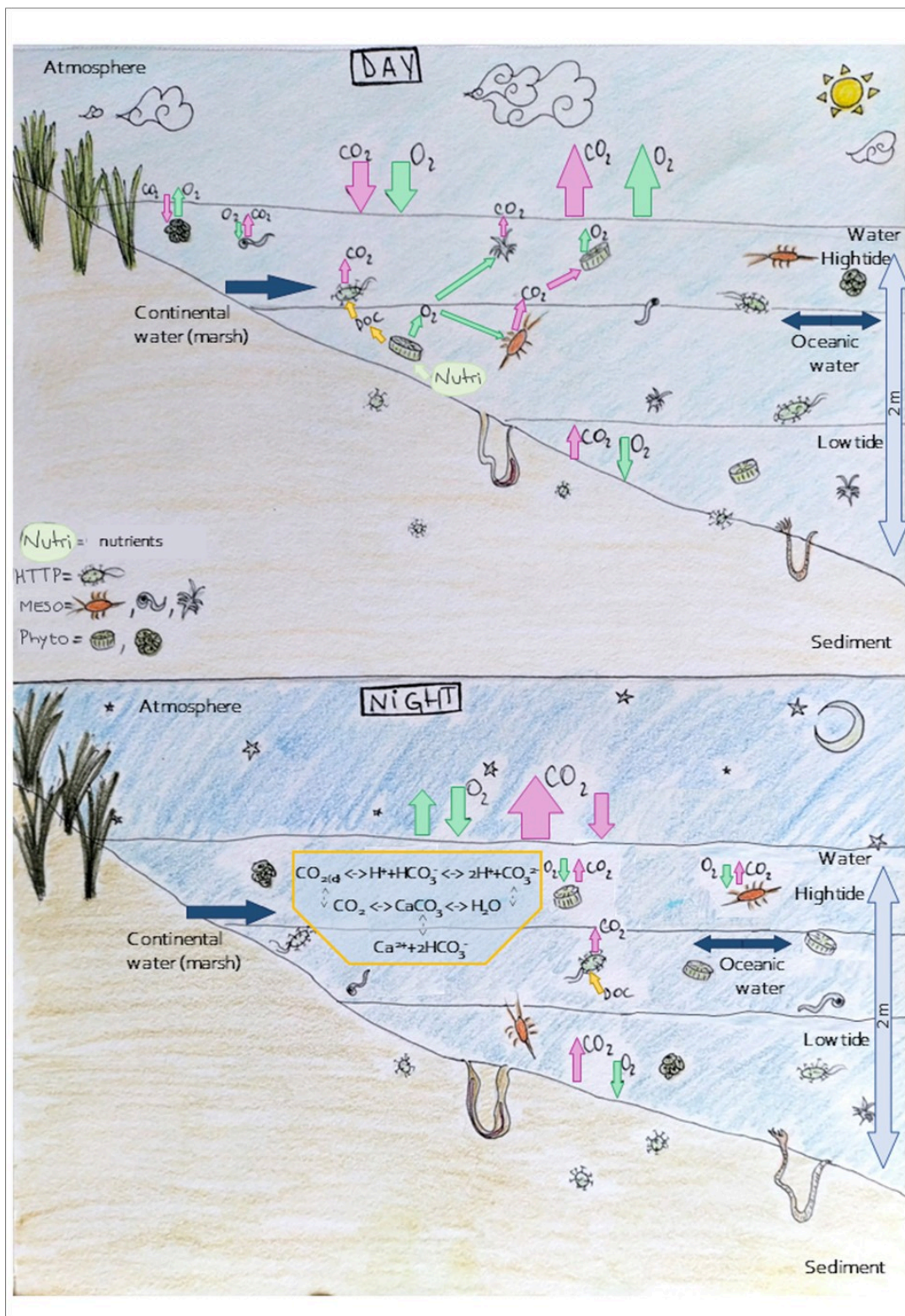
Figures

Figure 1

Conceptualized scheme of planktonic community CO_2 and O_2 exchanges during daytime and nighttime periods in the water column of a coastal environment (water height differences: 50 cm). DOC: dissolved organic carbon, Nutrients: NO_3^-, NO_2^-, PO_4^{3-}, NH_4^+, SI, HTTP: heterotrophic prokaryotes, Zoo: micro and mesozooplankton, Phyto: pico, nano, and microphytoplankton. The equations depict gas (CO_2/O_2) exchanges and gradients at the water-air interface, along with biological processes involving the

carbonate system (dissolved CO_2 $CO_{2(d)}$, bicarbonate ions HCO_3^-, carbonate ions CO_3^{2-} and calcium carbonate $CaCO_3$) through photosynthesis/respiration and $CaCO_3$ dissolution/precipitation. Illustration by L. Xaus
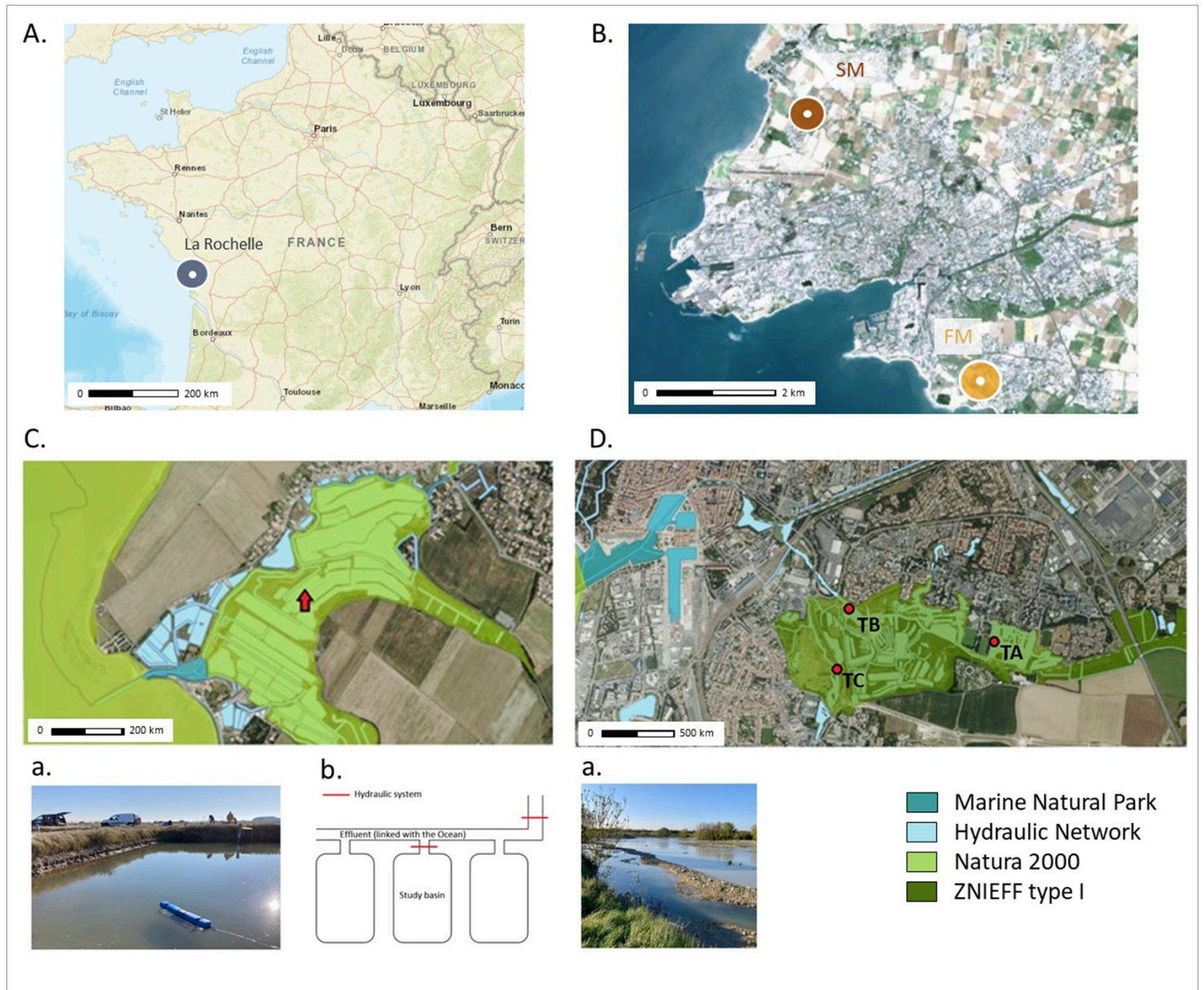
Figure 2

(A) Location of the La Rochelle metropolitan area on the westAtlantic French coast. (B) Location of L'Houmeau (SM) and Tasdon (FM) within the La Rochelle metropolitan area. (C) Experimental site of the L'Houmeau saltwater marsh (SM). The red arrow in the satellite image (geoportal) indicatesthe location of the studied basin (46°12'17.4"N 1°11'41.3"W). Lightblue lines represent the hydraulic network and water pathwaysbetween the marsh and sea waters. Thedark blue areas denote a small fraction of the Marine Natural Park, and thegreen areas indicate the Natura 2000 site. The studied basin is shown in (C, a) with autonomously deployed water probes. (C, b) Represents the hydraulic system. (Moncelon, 2022; photo: Polseneare Pierre). (D) Satellite image from the geoportal of Tasdon's freshwater marsh (FM) (D,

a). Light blue lines represent the hydraulic network and water pathwaysbetween the marsh and seawaters. Darkblue areas indicate a small fraction of the Marine Natural Park, and green areas represent a ZNIEFF type I. StationsTA, TB and TC (46°8'56.4" N, 1°7'26.4" W; 46° 9'3.6" N, 1°8'9.6" W; 46° 8'49.2" N, 1°8'13.2" W respectively) are marked by red points. (D, a) Images from stations TA (photo: Pierre Polsenaere)
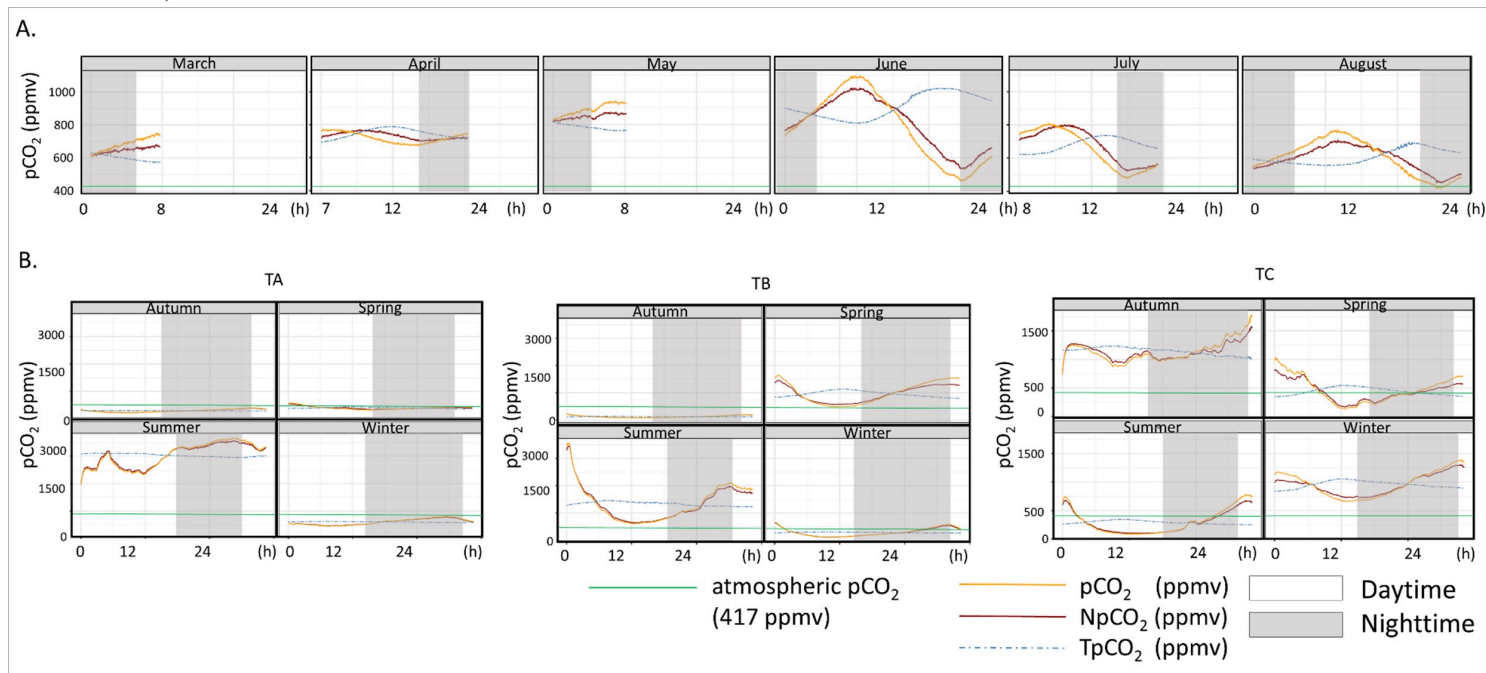

Figure 3

Variations in water pCO_2 (water CO_2 partial pressure; orange line), $TpCO_2$ (temperature effects on pCO_2 variations; dotted blue line), and $NpCO_2$ (non-temperature effects on pCO_2 variations; dark red line) measured over a 24-hour period (0, 12, 24 hours) at each marsh site and season. (A) Monthly variations in the L'Houmeau saltwater marsh (SM). Missing data at the SM correspond to faulty equipment. (B) Stations in the Tasdon freshwater marsh (FM) (from left to right: TA, TB, and TC) by season. Atmospheric pCO_2 value is represented by the green line
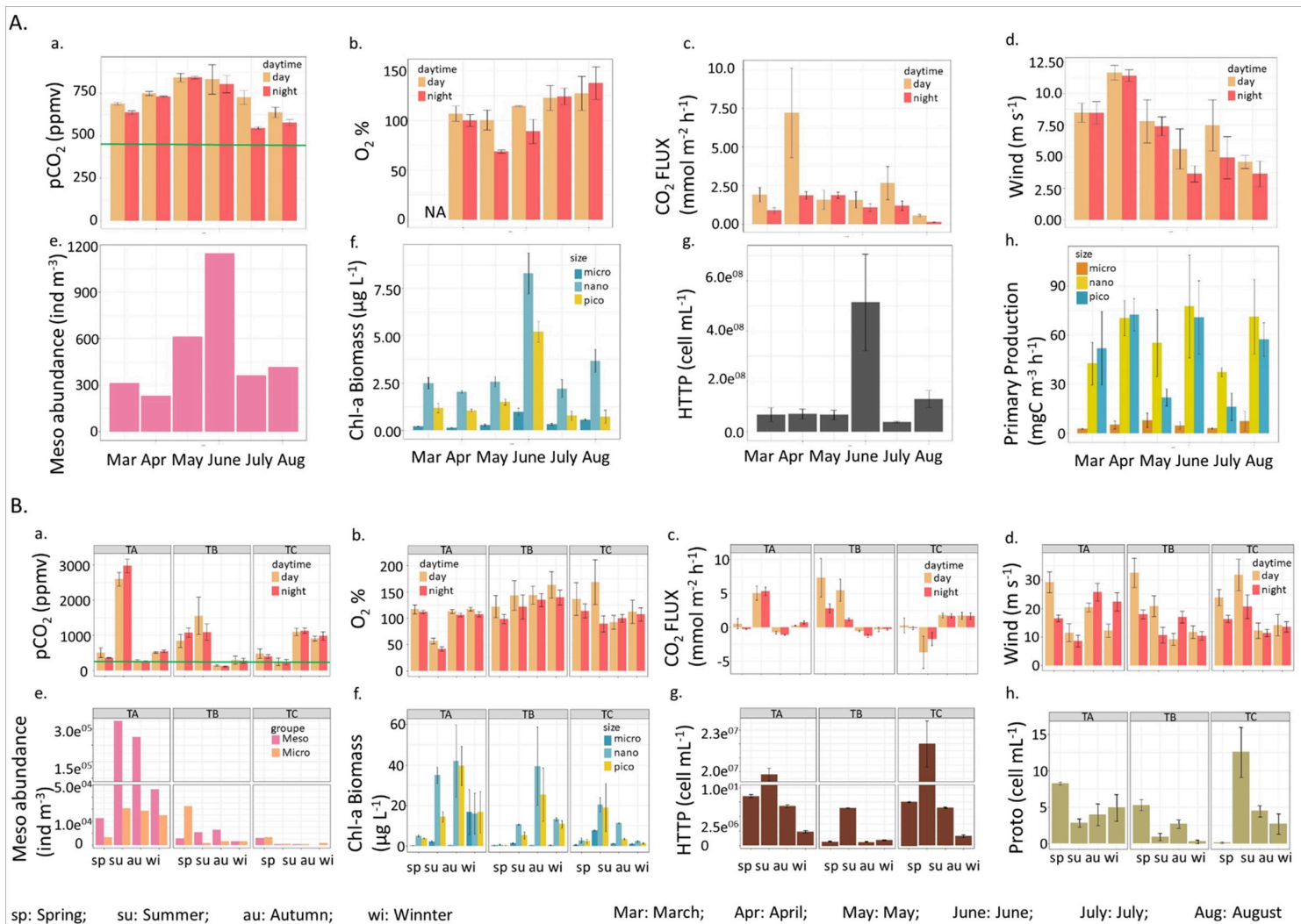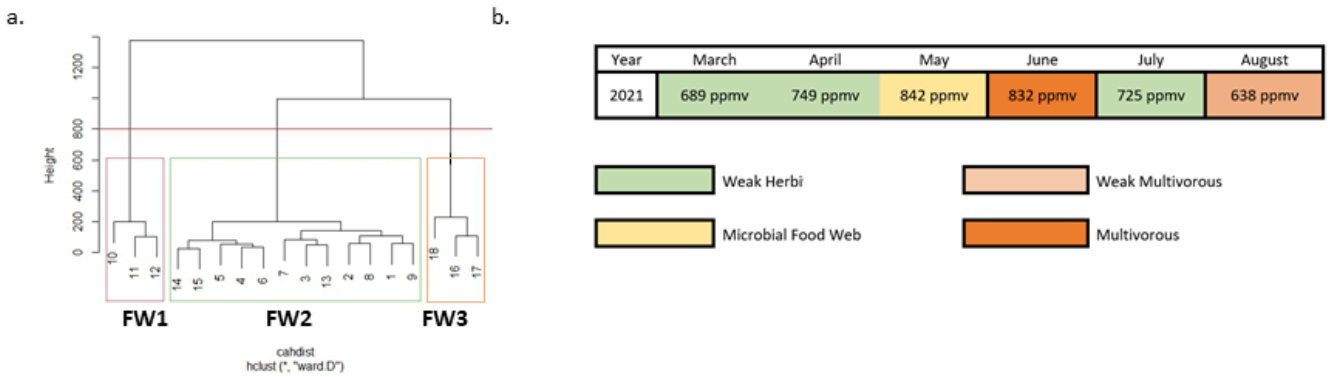
Figure 4

(A) Biotic variables measured at the L'Houmeau saltwater marsh (SM) (monthly measurements between March and August 2021); and (B) the Tasdon freshwater marsh (FM) (seasonal measurements at stations A, B, and C). (a) Water CO_2 partial pressure (ppmv), (b) O_2 % saturation, (c) estimated water-air CO_2 flux (mmol m^{-2} h^{-1}), (d) wind speed (m s^{-1}), (e) Meso abundance (individuals m^{-3}); (f) Chl$a$ biomass (µg L^{-1} ± sd) by size class (micro: microphytoplankton (>20 µm), nano: nanophytoplankton (3-20 µm) and pico: picophytoplankton (< 3 µm)), and (g) HTTP abundance (cells mL^1). (A, h) Chl$a$ PP by fraction (mg C m^{-3} h^{-1}) (micro, nano, pico) (mean ± sd) and (B, h) Heterotrophic protozoan (cell mL^{-1} ± sd). Atmospheric pCO$_2$ value is represented by the green horizontal line (417 ppmv; A, a and B, a)
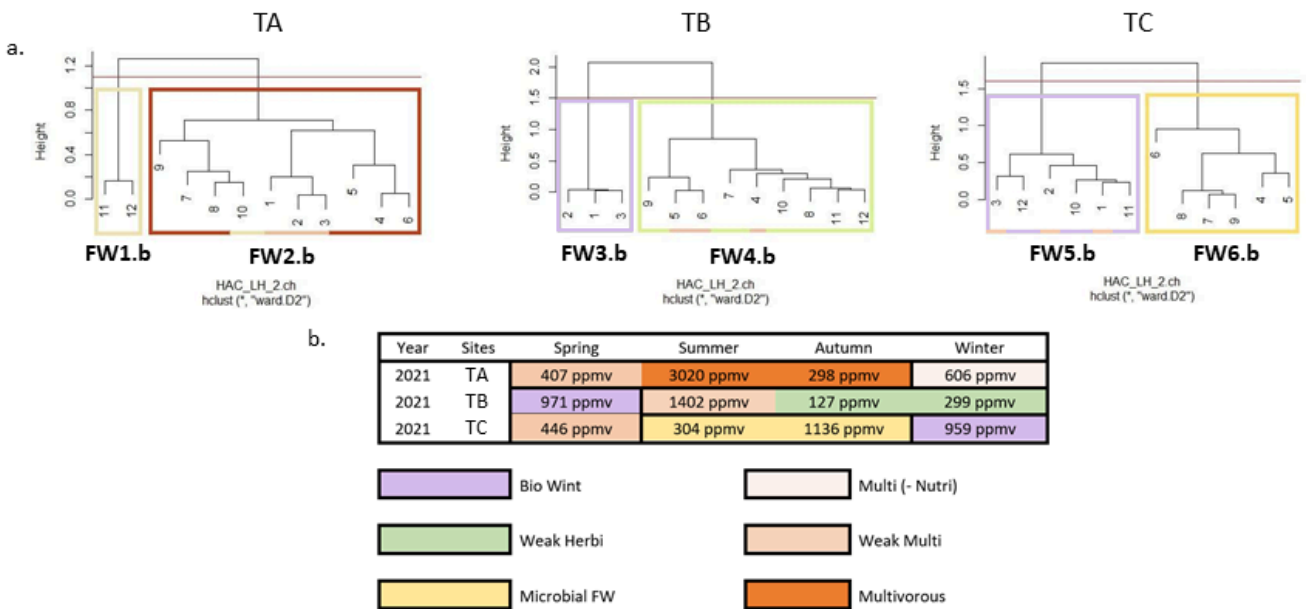
Figure 5

Clustering dendrograms for the HAC (hierarchical agglomerative clustering) applied to the biological matrix at (A, a) the L'Houmeau saltwater marsh (SM), with different food webs (FW1, FW2, FW3) defined by the cutting method "Ward.D1" (red line). Each number represents a replicate (1 to 3: March (FW2), 4 to 6: April (FW2), 7 to 9: May (FW2), 10 to 12: June (FW1), 13 to 15: July (FW2), 16 to 18: August (FW3); and (B, a) the Tasdon freshwater marsh (FM) stations (TA, TB, TC). There are two different food webs per station defined by the cutting method "Ward.D2" (red line). Each number represents a replicate (1 to 3: spring, 4 to 6 summer, 7 to 9: autumn, 10 to 12: winter), and colors indicate food web topology (FW1.b, FW2.b, FW3.b, FW4.b, FW5.b, FW6.b). Lastly, the association of food webs with either (A, b) monthly or (B, b) seasonal pCO$_2$ values is shown (A and B, b)
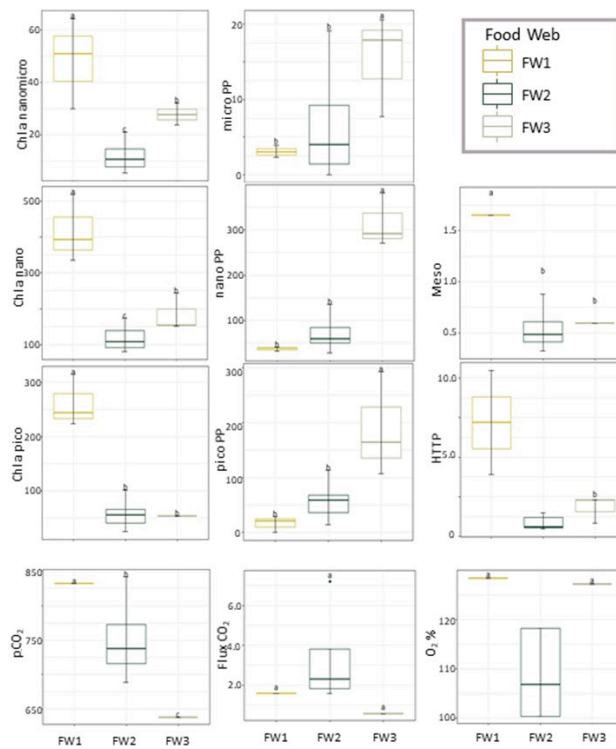
Figure 6

Box plots displaying the mean per food web type for Chl*a* (Chlorophyll-*a*) by size class, Meso (Mesozooplankton), HTTP (Heterotrophic prokaryote), and PP (Chl*a* primary production) by fraction used for the Hierarchical Agglomeration Clustering analysis at the SM (L'Houmeau saltwater marsh). Box plot labeled with the same letters are not significantly different (ANOVA followed by Fisher's LSD). All biotic variables have the same unit (μg C L^{-1}) but scales were different. In addition, *box plots* with water CO_2 partial pressure (pCO_2, ppmv), CO_2 flux (mmol m^{-2} h^{-1}), and O_2 saturation % (%) mean per food web were added
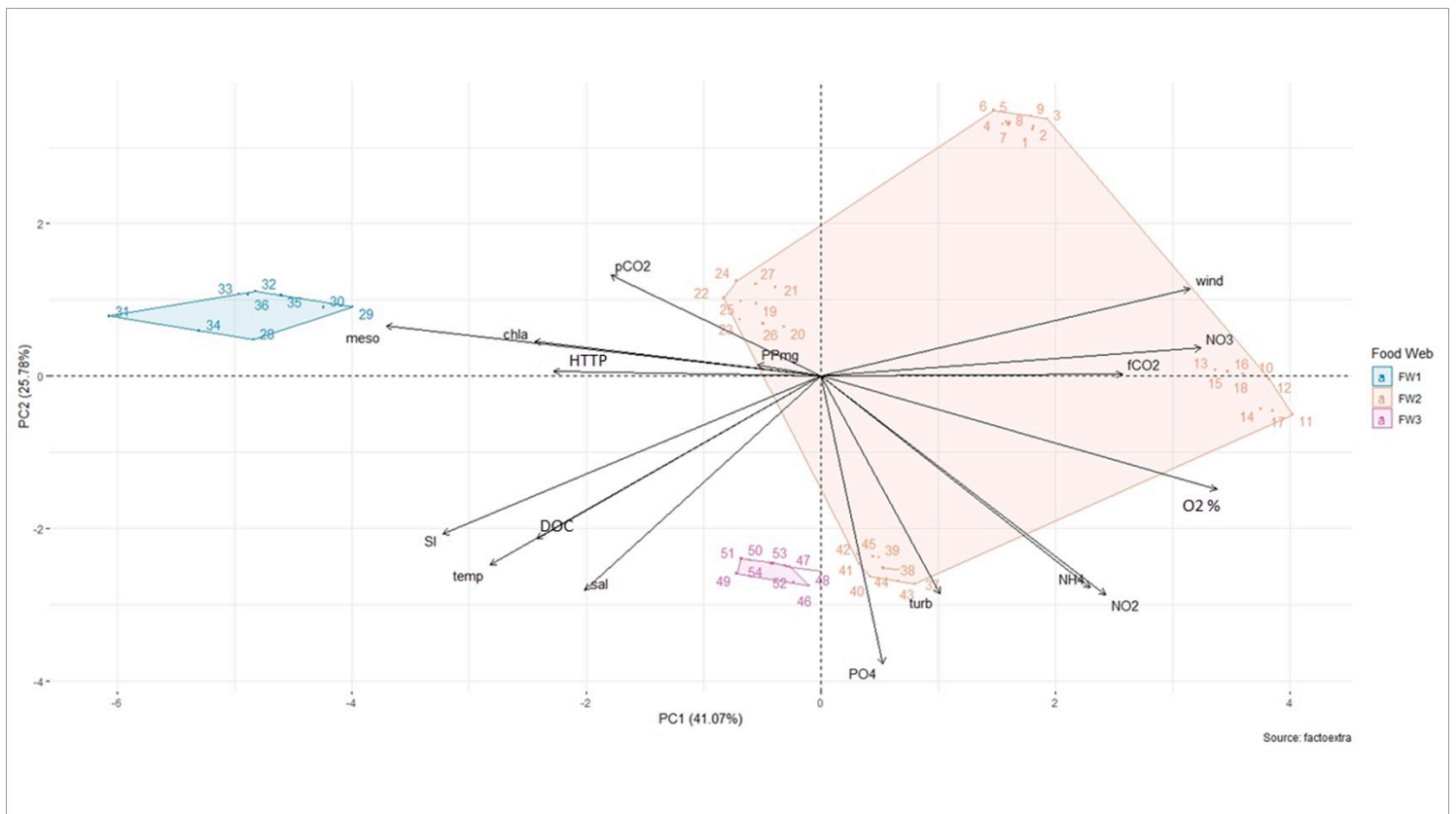
Figure 7

Principal Component Analysis at the SM (L'Houmeau saltwater marsh) between March 2021 and August 2021 of abiotic parameters: temperature (temp, °C), salinity (Sal), turbidity (Turb, NTU), O_2% (%), water pCO_2 (ppmv), water-air CO_2 fluxes (fCO_2, mmol m^{-2} h^{-1}), wind gust (wind, m s^{-1}), DOC (mg L^{-1}), NO_3^-, NO_2^-, NH_4^+, PO_4^{3-}, Si (µmol L^{-1})) and biotic parameters: Chl*a* biomass (Chlorophyll-*a*, µg L^{-1}), PP (Chl*a* primary production, mg C m^{-3} h^{-1}), Meso (mesozooplankton, individuals m^{-3}) and HTTP (Heterotrophic prokaryote, cells mL^{1}). Food web (FW) types are represented by different colors, and months by group of numbers (1 to 9: March, 10 to 18: April, 19 to 27: May, 28 to 36: June, 37 to 45: July, 46 to 54: August)
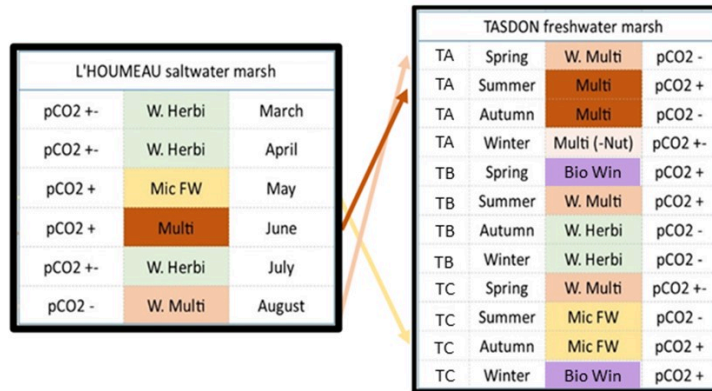
Figure 8

Relationships (arrows) between food webs and water pCO_2 in studied coastal marshes (Tasdon FM and L'Houmeau SM)